AGU PUBLICATIONS

Global Biogeochemical Cycles

RESEARCH ARTICLE
10.1002/2015GB005146

Key Points:
- Isotopic composition of TGM differed among meteorologically identified sources
- Background atmospheric TGM displayed moderately positive δ^{202}Hg values
- Anthropogenic emissions drive TGM isotopic composition to lower δ^{202}Hg values

Supporting Information:
- Figure S1 and Table S1

Correspondence to:
J. D. Demers,
jdemers@umich.edu

Citation:
Demers, J. D., L. S. Sherman, J. D. Blum, F. J. Marsik, and J. T. Dvonch (2015), Coupling atmospheric mercury isotope ratios and meteorology to identify sources of mercury impacting a coastal urban-industrial region near Pensacola, Florida, USA, *Global Biogeochem. Cycles*, *29*, 1689–1705, doi:10.1002/2015GB005146.

Received 15 MAR 2015
Accepted 14 SEP 2015
Accepted article online 18 SEP 2015
Published online 16 OCT 2015

Coupling atmospheric mercury isotope ratios and meteorology to identify sources of mercury impacting a coastal urban-industrial region near Pensacola, Florida, USA

Jason D. Demers[1], Laura S. Sherman[1], Joel D. Blum[1], Frank J. Marsik[2], and J. Timothy Dvonch[2]

[1]Department of Earth and Environmental Sciences, University of Michigan, Ann Arbor, Michigan, USA, [2]Air Quality Laboratory, University of Michigan, Ann Arbor, Michigan, USA

Abstract Identifying the anthropogenic and natural sources of mercury (Hg) emissions contributing to atmospheric mercury on local, regional, and global scales continues to be a grand challenge. The relative importance of various direct anthropogenic emissions of mercury, in addition to natural geologic sources and reemission of previously released and deposited mercury, differs regionally and temporally. In this study, we used local-scale, mesoscale, and synoptic-scale meteorological analysis to couple the isotopic composition of ambient atmospheric mercury with potential sources of mercury contributing to a coastal urban-industrial setting near a coal-fired power plant in Pensacola, Florida, USA. We were able to broadly discern four influences on the isotopic composition of ambient atmospheric mercury impacting this coastal urban-industrial region: (1) local to regional urban-industrial anthropogenic emissions (mean δ^{202}Hg = 0.44 ± 0.05‰, 1SD, n = 3), (2) marine-influenced sources derived from the Gulf of Mexico (mean δ^{202}Hg = 0.77 ± 0.15‰, 1SD, n = 4), (3) continental sources associated with north-northwesterly flows from within the planetary boundary layer (mean δ^{202}Hg = 0.65 ± 0.04‰, 1SD, n = 3), and (4) continental sources associated with north-northeasterly flows at higher altitudes (i.e., 2000 m above ground level; mean δ^{202}Hg = 1.10 ± 0.21‰, 1SD, n = 8). Overall, these data, in conjunction with previous studies, suggest that the background global atmospheric mercury pool is characterized by moderately positive δ^{202}Hg values; that urban-industrial emissions drive the isotopic composition of ambient atmospheric mercury toward lower δ^{202}Hg values; and that air-surface exchange dynamics across vegetation and soils of terrestrial ecosystems drive the isotopic composition of ambient atmospheric mercury toward higher positive δ^{202}Hg values. The data further suggest that mass-independent fractionation (MIF) of both even-mass- and odd-mass-number isotopes, likely generated by photochemical reactions in the atmosphere or during reemission from terrestrial and aquatic ecosystems, can be obscured by mixing with anthropogenic emissions having different MIF signatures.

1. Introduction

Identifying the anthropogenic and natural sources of mercury (Hg) emissions contributing to atmospheric mercury on local, regional, and global scales is challenging. Globally, the primary sources of anthropogenic mercury emissions to the atmosphere include fossil fuel combustion (primarily coal); artisanal and small-scale gold mining; mining, smelting, and production of metals; and cement production [*Pacyna et al.*, 2006; *Selin and Jacob*, 2008; *Selin*, 2009; *Telmer and Veiga*, 2009; *Pirrone et al.*, 2010; *United Nations Environment Program (UNEP)*, 2013]. Although the United Nations Environment Program recently ranked artisanal and small-scale gold mining (37%) ahead of coal burning (24%) in contributions of mercury to the global atmosphere [*UNEP*, 2013], the relative importance of these sources differs regionally and temporally, based in part on socioeconomic factors, development and implementation of control technologies, and regulatory action [*Pirrone et al.*, 2010]. For example, in the United States, prior to the U.S. Environmental Protection Agency (USEPA) Mercury and Air Toxics Standards ruling that may eventually require ~90% reductions in power plant emissions of mercury [*U.S. Environmental Protection Agency*, 2014b], coal combustion remained responsible for ~50% of all anthropogenic emissions of mercury in the United States [*Pirrone et al.*, 2009]. Moreover, in the southeastern U.S. where this study took place, electricity generation (primarily coal combustion) and iron and steel manufacturing are the dominant anthropogenic sources of mercury emissions (Figure 1)

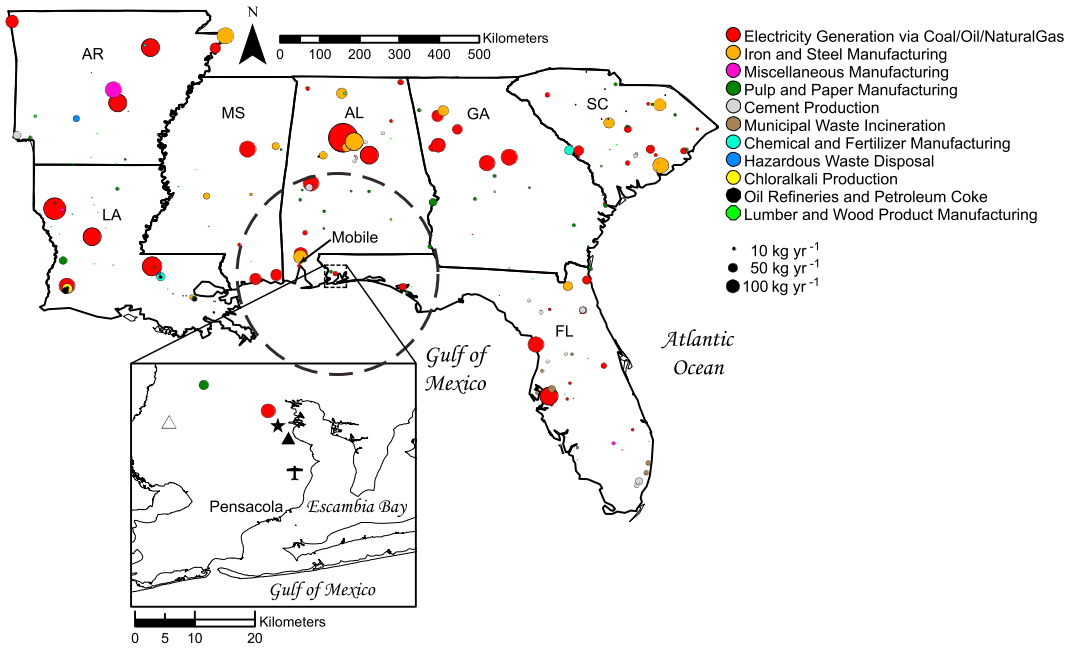

Figure 1. Map of sampling location for ambient atmospheric mercury (total gaseous mercury, TGM) in a coastal urban-industrial region near a coal-fired power plant in Pensacola, Florida, and emissions of total mercury (THg; kg yr^{-1}) in the southeastern region of the United States, including Arkansas (AR), Louisiana (LA), Mississippi (MS), Alabama (AL), Georgia (GA), South Carolina (SC), and Florida (FL) [*U.S. Environmental Protection Agency (USEPA),* 2011b]. Mercury emissions source categories are differentiated by color; circles are scaled by radius to represent the magnitude of annual emissions from each source. The dashed circle centered in Pensacola shows the region within 250 km of the TGM sampling site. The inset shows the sampling location in Pensacola, Florida: the black star shows the location of the 30 consecutive 24 h daily TGM samples; the black triangle shows the location of the Florida Department of Environmental Protection Air Quality Monitoring site for criteria pollutants (e.g., SO_2); the white triangle shows the location of the speciated atmospheric mercury concentration monitoring site; and the airplane symbol shows the location of the Pensacola International Airport where local-scale meteorological conditions are monitored [*NOAA*, 2014a]. The red circle within the inset shows the location of the Gulf Power Company's James F. Crist coal-fired power plant (19.9 kg yr^{-1} THg); the green circle within the inset shows the location of a local International Paper Company pulp and paper manufacturing facility (9.3 kg yr^{-1} THg); the size of the symbols within the inset are not scaled relative to annual emissions.

[*USEPA*, 2011b]. In addition to direct anthropogenic emissions of mercury, natural geologic sources and re-emission of previously released and deposited mercury account for ~73% of global fluxes to the atmosphere [*Selin and Jacob*, 2008; *Selin*, 2009; *Pirrone et al.*, 2010; *Amos et al.*, 2013; *UNEP*, 2013], with terrestrial ecosystems accounting for ~25% and oceans accounting for ~45% [*Selin and Jacob*, 2008; *Selin*, 2009]. Whereas emissions estimates have been used to quantify point source anthropogenic releases of mercury to the atmosphere, assessing the geographic extent of the impact of emissions and reemissions is more difficult, due in part to atmospheric mixing and complex atmospheric chemistry.

The form of mercury emitted to the atmosphere influences its transport and deposition. Mercury is emitted in three forms: (1) divalent reactive gaseous oxidized mercury (GOM, $Hg(II)_{(g)}$), (2) particulate-bound mercury associated with aerosols (PBM, $Hg(II)_{(p)}$), and (3) gaseous elemental mercury (GEM, $Hg(0)_{(g)}$). Whereas natural emissions are primarily GEM, anthropogenic emissions can include a much higher percentage of oxidized species (GOM, PBM). For example, mercury speciation in coal combustion flue gases is influenced by coal characteristics, combustion conditions, and control technologies [*Srivastava et al.*, 2006; *Wilcox et al.*, 2012; *Zhang et al.*, 2013b; *Sporl et al.*, 2014; *Ticknor et al.*, 2014], resulting in stack emissions that are typically composed of 50–80% GOM, <5% PBM, and 20–50% GEM [*Carpi*, 1997] but can vary widely (3–83% GOM, 0.1–40% PBM, and 16–97% GEM) [*U.S. Environmental Protection Agency (USEPA)*, 2011a]. GOM is rapidly stripped from the atmosphere and deposited locally in wet and dry deposition, whereas PBM can be transported more regionally, and GEM can be transported globally before being oxidized during atmospheric and surface reactions and deposited [*Keeler et al.*, 1995; *Lindberg and Stratton*, 1998; *Schroeder and Munthe*, 1998]. As a result, atmospheric mercury is mainly composed of GEM (>95%) [*Lindberg and Stratton*, 1998].

Various approaches have been used to better understand local and regional sources of mercury emissions contributing to both wet and dry deposition. Monitoring networks have provided long-term records that show broad regional deposition patterns (e.g., Mercury Deposition Network and Atmospheric Mercury Network) [*Butler et al.*, 2008]. Measurements of mercury speciation (GOM, PBM, and GEM) in ambient atmospheric samples have provided critical information for species-specific modeling of transport and dry deposition. Trace metal analysis, meteorological assessments, multivariate statistical receptor models, and combinations thereof have been applied to assess local and regional source-receptor relationships [*Dvonch et al.*, 1999; *Landis and Keeler*, 2002; *Graney et al.*, 2004; *Dvonch et al.*, 2005; *Gratz and Keeler*, 2011; *Gratz et al.*, 2013a, 2013b]. Recently, analysis of mercury stable isotope ratios in wet deposition and ambient atmospheric samples has begun to add additional insight into source identification and the processes affecting mercury during atmospheric transport [*Gratz et al.*, 2010; *Chen et al.*, 2012; *Sherman et al.*, 2012; *Demers et al.*, 2013; *Rolison et al.*, 2013; *Zhang et al.*, 2013a; *Fu et al.*, 2014; *Sherman et al.*, 2015]. Nonetheless, there remains a need to better constrain the isotopic composition of both natural and anthropogenic emissions of mercury to the atmosphere and the global atmospheric mercury reservoir.

The seven stable isotopes of Hg (196, 198–202, and 204 amu) can be fractionated both mass dependently (MDF) and mass independently (MIF). Mercury isotope ratios are reported using delta notation relative to a common standard reference material (see section 2.4) [*Blum and Bergquist*, 2007]. Mass-dependent fractionation can occur under both kinetic and equilibrium processes, and during both biotic and abiotic reactions. Mass-independent fractionation of the odd-mass-number isotopes of Hg occurs primarily during photochemical reactions due to the magnetic isotope effect (MIE) [*Bergquist and Blum*, 2009]. Recent studies have also observed MIF of even-mass-number isotopes of Hg in precipitation and ambient atmospheric samples [*Gratz et al.*, 2010; *Chen et al.*, 2012; *Sherman et al.*, 2012; *Demers et al.*, 2013; *Wang et al.*, 2015]. Although the mechanism resulting in even-mass-number MIF remains unclear, it may be the result of nuclear volume effects (NVE) or nuclear self-shielding and could be indicative of upper atmospheric processes [*Gratz et al.*, 2010; *Chen et al.*, 2012].

Industrial processes can influence the isotopic composition of ambient atmospheric mercury. For example, mercury emissions from coal-fired power plants can be fractionated relative to the original isotopic composition of combusted coal. *Sun et al.* [2013] modeled fractionation within a coal-fired utility boiler equipped with electrostatic precipitators (ESPs) and suggested that bulk stack emissions are enriched by an average of ~0.3‰ in δ^{202}Hg relative to feed stocks. They concluded that emitted GEM was likely enriched in heavier isotopes and GOM was likely enriched in lighter isotopes of Hg [*Sun et al.*, 2013, 2014]. Such fractionation may be recorded in the isotopic composition of ambient atmospheric mercury that is impacted by industrial sources. In fact, *Gratz et al.* [2010] showed that air derived from urban-industrial regions of the northern Midwest USA had δ^{202}Hg values that were more negative than those associated with air transported across rural regions.

Finally, natural environmental processes can also modify the isotopic composition of ambient atmospheric mercury. For example, *Demers et al.* [2013] showed that interaction of total gaseous mercury (TGM) with vegetation can result in fractionation that drives the atmospheric TGM pool to highly positive δ^{202}Hg values, likely due to the oxidation of GEM within stomatal cavities. Such air-surface exchange processes could also influence the isotopic composition of ambient atmospheric mercury passing over marine environments, as could evasion or photochemical reduction from marine or terrestrial ecosystems. Reduction and oxidation processes in the atmosphere, likely involving photochemical mechanisms, also result in fractionation between GEM and GOM pools [e.g., *Chen et al.*, 2012].

Although the study of mercury isotope dynamics of the global atmosphere is still in its infancy, results to date indicate that mercury isotopes may prove useful for identifying sources and better understanding mercury cycling. Whereas there is some indication of the variability in isotopic composition of ambient atmospheric mercury at predominantly background sites that are not impacted by urban-industrial emissions [*Gratz et al.*, 2010; *Demers et al.*, 2013; *Fu et al.*, 2014], only two urban-industrial influenced Hg isotope measurements have been reported previously [*Gratz et al.*, 2010]. Thus, the objective of this study was to identify the isotopic composition associated with sources of ambient atmospheric mercury impacting a complex coastal urban-industrial region near a coal-fired power plant in Pensacola, Florida (FL), USA. Herein, we accomplish this goal by coupling a 30 day temporally resolved record of mercury isotopic composition in

ambient atmospheric samples with meteorological assessments and analysis of criteria pollutants that allow us to identify local, regional, and global sources that potentially contribute mercury to this near-coastal site.

2. Methods

2.1. Site Description

Ambient atmospheric mercury samples were collected in Pensacola, FL, in an open field on the campus of the University of West Florida (30.5453°N, −87.2119°W) during a 30 day period from 24 July to 22 August 2010 (Figure 1). This site was located adjacent to Escambia Bay and within 25 km of the Gulf of Mexico. The largest local sources of anthropogenic emissions of mercury included the Gulf Power Company James F. Crist coal-fired power plant located 2.7 km to the northwest (19.9 kg yr^{-1}) and an International Paper Company pulp and paper mill located 12.5 km to the northwest (9.3 kg yr^{-1}) [*USEPA*, 2011b]. Larger local- to regional-scale sources of anthropogenic emissions including coal-fired power plants and steel manufacturing facilities were concentrated to the west near Mobile, Alabama (<100 km west, ~270.2 kg yr^{-1}), and along the Gulf Coast of Mississippi (<200 km west, ~155.0 kg yr^{-1}). Broader-scale regional emission sources across the southeastern USA were also dominated by electricity generation via fossil fuel combustion (predominantly coal) and iron and steel manufacturing. Thus, this sampling site represents a complex setting potentially impacted by both marine-derived air and a mixture of local and regional anthropogenic sources of mercury.

2.2. Sample Collection

Atmospheric total gaseous mercury (TGM = GEM + GOM) samples for isotopic analysis were collected approximately 3 m above ground level using methods described in *Demers et al.* [2013]. Although the speciation and isotopic composition of mercury from various sources and processes can differ, our species-integrated TGM isotopic measurements are indicative of the overall influence of different source signatures impacting the sampling site during each sampling period. The isotopic composition of separated GEM and GOM could be additionally informative; however, techniques for the collection of adequate masses of GOM (typically < 5% of TGM [*Lindberg and Stratton*, 1998]) for isotopic analysis have not yet been sufficiently developed. Samples were collected by drawing air through eight gold-coated bead traps deployed in parallel via a PVC manifold at an average rate of 2.3 L min^{-1} per trap for 22.1 ± 1.7 h (1SD). All traps were heated to ~500°C to remove mercury and then blank checked prior to use. Flow was drawn through the traps using a single electric pump, and total flow was recorded with a dry test meter (DTM). Coarse particulates were removed from the sample stream at the inlet to each trap with a quartz fiber filter (Whatman QMA 47mm disks, 0.7 μm nominal pore size). Prior to use, quartz fiber filters were ashed in a muffle furnace at 750°C for 6 h. To prevent condensation within the gold-coated bead traps, the traps were heated to 55°C during sample collection. After sample collection, loaded traps were capped, wrapped with Teflon tape, triple bagged, and sealed in a clean cooler. In conjunction with another ongoing study in the Pensacola region, Tekran speciated mercury analyzers (Model #2537/1130/1135) that measured GEM and GOM concentrations at hourly intervals were deployed in an outlying field ~15 km west of our study site (Figure 1). From these data, we calculated daily mean atmospheric concentrations of GEM and GOM to compare with daily mean TGM concentrations collected on gold-bead traps for isotopic analysis.

2.3. Sample Desorption and Concentration Analysis

Atmospheric TGM samples collected on gold-coated bead traps in the field were concentrated into an oxidizing solution of 1% $KMnO_4$ (weight/weight) in 10% sulfuric acid (vol/vol) (hereafter, referred to as 1% $KMnO_4$) through a multistep process as described in *Demers et al.* [2013]. In brief, each trap was dried for 1 h in a stream of Hg-free Argon gas at 0.5 L min^{-1} and then flash heated to ~500°C under a 0.5 L min^{-1} flow of gold-filtered clean room air to release mercury onto a secondary analytical gold-coated sorbent trap. Use of a backup trap and real-time monitoring verified that breakthrough was negligible. The secondary analytical trap was then thermally desorbed into a 24 g 1% $KMnO_4$ trapping solution by slowly heating to 550°C over 3.5 h in a gold-filtered Argon gas stream (8 mL min^{-1}). A small aliquot of this solution was analyzed for concentration in order to calculate the total quantity of mercury collected. Average atmospheric TGM concentration (ng m^{-3}) for each sampling period was determined by dividing total mercury mass (ng) by total volume of air sampled (m^3), as recorded using DTMs. The mercury in this 1% $KMnO_4$ solution was then concentrated into a secondary 1% $KMnO_4$ solution via purge and trap [see *Demers et al.*, 2013], resulting in final

concentrations ranging from 2.5 to 4.2 ppb for isotope analysis. The performance of the desorption procedure was monitored with procedural blanks and standards. Procedural blanks were composed of a set of eight traps that were installed in the sampling manifold in the field and then removed and repackaged without pumping ambient air across them. Procedural blanks ranged from 0.16 to 0.18 ng Hg ($n = 2$), representing a maximum of 1% of any sample Hg mass. Each set of eight traps for each procedural standard was loaded with 30 ng Hg (3.75 ng per trap; National Institute of Standards and Technology Standard Reference Material (NIST SRM) 3133), similar to the amount of TGM collected during field sampling (17–32 ng Hg per sample). Recovery of procedural standards was monitored for both the initial desorption and the secondary preconcentration step: recovery during initial desorption ranged from 92.3 to 96.4% (93.9 ± 1.6%, 1SD, $n = 8$); recovery during secondary preconcentration ranged from 95.5% to 102.2% (98.4 ± 2.2%, 1SD, $n = 8$). This resulted in an overall procedural recovery ranging from 89.0% to 94.5% (92.4% ± 1.8%, 1SD, $n = 8$).

2.4. Mercury Isotope Analysis

Atmospheric TGM samples were concentrated into 1% $KMnO_4$ solution and analyzed for isotopic composition with a multiple collector inductively coupled plasma mass spectrometer (Nu Instruments) using continuous flow cold vapor generation with Sn(II) reduction [*Blum and Bergquist*, 2007]. We employed an arrangement of faraday cups that allows for simultaneous collection of masses 196, 198, 199, 200, 201, 202, 203, 204, 205, and 206. Instrumental mass bias was corrected using an internal standard (NIST SRM 997, $^{205}Tl/^{203}Tl$ ratio of 2.38714) and strict sample-standard bracketing with NIST SRM 3133 Hg standard. Isobaric interferences from ^{204}Pb were monitored to allow correction using mass 206; however, they were always negligible. On-peak zero corrections were applied to all masses.

Samples stabilized in 1% $KMnO_4$ were prereduced with 30% hydroxylamine hydrochloride. Standard concentrations were matched to within 5% of sample concentrations. Mercury in sample solutions was reduced online with 2% $SnCl_2$ [*U.S. Environmental Protection Agency*, 1998], and the mixed solution was delivered to a phase separator. Reduced mercury was stripped from solution with a counterflow of Ar into which a dry Tl aerosol was introduced using a desolvating nebulizer (Aridus, Cetac). We report isotopic compositions as per mil (‰) deviations from the average of NIST SRM 3133 bracketing standards using delta notation:

$$\delta^{xxx}\mathrm{Hg}\ (‰) = \left\{\left[\left(^{xxx}\mathrm{Hg}/^{198}\mathrm{Hg}\right)_{\mathrm{unknown}} / \left(^{xxx}\mathrm{Hg}/^{198}\mathrm{Hg}\right)_{\mathrm{NIST\ SRM\ 3133}}\right] - 1\right\} \times 1000 \quad (1)$$

where *xxx* is the mass of each mercury isotope between ^{199}Hg and ^{204}Hg. We use $\delta^{202}Hg$ to report MDF. MIF is reported as the deviation of the isotope ratio from the theoretically predicted values based on the kinetic mass-dependent fractionation law and measured $\delta^{202}Hg$ value [*Blum and Bergquist*, 2007]. MIF is reported in "capital delta" notation ($\Delta^{xxx}Hg$) (equation (2)) and is well approximated for small ranges in delta values (≤10‰) by equation (3):

$$\Delta^{xxx}\mathrm{Hg}\ (‰) = 1000 \times \left(\left\{\ln\left[\left(\delta^{xxx}\mathrm{Hg}/1000\right) + 1\right]\right\} - \beta \times \left\{\ln\left[\left(\delta^{202}\mathrm{Hg}/1000\right) + 1\right]\right\}\right) \quad (2)$$

$$\Delta^{xxx}\mathrm{Hg}\ (‰) \approx \delta^{xxx}\mathrm{Hg} - \left(\delta^{202}\mathrm{Hg} \times \beta\right) \quad (3)$$

where *xxx* is the mass of each mercury isotope 199, 200, 201, 204 and β is a constant (0.252, 0.502, 0.752, and 1.492, respectively) [*Blum and Bergquist*, 2007].

We characterized the uncertainty of mercury isotope measurements using a secondary standard (UM-Almaden) and procedural standards [*Blum and Bergquist*, 2007]. To characterize the reproducibility of the mass spectrometry, we measured the isotopic composition of UM-Almaden several times (5–7) at representative high and low concentrations within each analytical session. The 2SD uncertainty was then generated from the average of session averages for each delta value; there was no difference in the reproducibility for concentrations ranging from 2.5 to 4.2 ppb during the analytical sessions reported in this study. For TGM procedural standards, we calculated uncertainty as 2SE of the average of session averages. We represent the uncertainty of samples with the uncertainty of procedural standards; however, where the 2SE of procedural standards was less than the 2SD of UM-Almaden, we instead represent sample uncertainty using UM-Almaden. The uncertainties associated with the isotopic composition of UM-Almaden and TGM procedural standards are presented in Table 1.

2.5. Criteria Pollutants

Hourly criteria pollutant emissions (SO_2 and NO_x) from the Gulf Power Company James F. Crist coal-fired power plant were obtained from USEPA Air Markets Program Data [*U.S. Environmental Protection Agency*, 2014a].

Table 1. Mercury Isotopic Composition of UM-Almaden and Procedural Standards[a]

Standard Type	*n*	δ^{204}Hg (‰)	2σ (‰)	δ^{202}Hg (‰)	2σ (‰)	δ^{201}Hg (‰)	2σ (‰)	δ^{200}Hg (‰)	2σ (‰)	δ^{199}Hg (‰)	2σ (‰)	Δ^{204}Hg (‰)	2σ (‰)	Δ^{201}Hg (‰)	2σ (‰)	Δ^{200}Hg (‰)	2σ (‰)	Δ^{199}Hg (‰)	2σ (‰)
UM-Almaden	5	−0.86	0.04	−0.57	0.03	−0.45	0.05	−0.27	0.04	−0.15	0.04	0.00	0.03	−0.03	0.04	0.02	0.04	−0.01	0.04
TGM (NIST SRM 3133)	8	0.08	0.08	0.06	0.04	0.04	0.05	0.04	0.04	0.02	0.03	0.00	0.04	−0.01	0.03	0.01	0.02	0.01	0.02

[a]For UM-Almaden, *n* is the number of preparations (i.e., the number of session averages, with separate values for preparations at different concentrations within a session). For ambient atmospheric mercury (total gaseous mercury, TGM) procedural standards, *n* is the number of preparations of the material. The 2σ for UM-Almaden shows 2SD of the average of session averages, whereas the 2σ for TGM procedural standards shows 2SE of the average of session averages (see section 2.4).

Local atmospheric SO_2 concentrations were measured by the Florida Department of Environmental Protection Air Quality Monitoring at the Ellyson Industrial Park site located 2.5 km southwest of the TGM sampling site (Figure 1). Criteria pollutant emissions and ambient SO_2 concentrations were tested for correlation with measured concentration and isotopic composition of TGM samples.

2.6. Meteorology

Local-scale meteorological measurements including surface wind speed, wind direction, and daily precipitation were obtained from the Pensacola International Airport (Station #GHCND:USW00013899) [*NOAA*, 2014a] located 8 km south-southwest of our TGM collection site (Figure 1). Daily precipitation was also measured at the TGM sampling site on the campus of UWF. Hourly wind speed and wind direction measurements were binned and averaged to correspond directly with daily TGM sampling periods. The transport history of air arriving at the sampling site was assessed using 24 h back trajectories calculated using the NOAA Hybrid Single-Particle Lagrangian Integrated Trajectory (HYSPLIT) model with EDAS40 data (40 km, 3 h resolution) [*Draxler and Rolph*, 2010] and starting heights at half the mixed layer depth. Mixed layer depths were determined by the HYSPLIT program based upon the model input data used to determine the back trajectories. The mixed layer depth at 1300 CDT was used to represent the established daytime mixed layer, whereas the mixed layer depth at 0100 CDT was used to represent the established nocturnal mixed layer. Another set of back trajectories using starting heights of 2000 m were used to assess higher-altitude air transport. Synoptic-scale meteorological features (i.e., pressure systems and fronts) were characterized using surface meteorological maps [*NOAA*, 2014b, 2014c]. Meteorological analyses were coupled with mercury isotope data to constrain the isotopic composition of various sources of ambient atmospheric mercury impacting our study site.

3. Results and Discussion

3.1. Mercury Concentration and Isotopic Composition

3.1.1. Mercury Concentrations

The daily average atmospheric TGM concentrations that we measured using gold-coated bead traps at this coastal urban-industrial site ranged from 0.84 to 1.26 ng m^{-3} (mean = 1.11 ± 0.09 ng m^{-3} 1SD; Table 2), thus varying by a factor of ~1.5. This was similar to daily atmospheric GEM concentrations (mean = 1.20 ± 0.06 ng m^{-3} 1SD) calculated from Tekran speciated mercury analyzers. Concentrations of GOM (0.38 ± 0.36 pg m^{-3} 1SD) were < 0.1% of GEM concentrations. The range in TGM concentrations based on gold-bead traps makes it plausible that additions of mercury (as much as ~50% or more) from local and regional sources could significantly shift the isotopic composition of the background atmospheric TGM pool. However, changes in TGM concentration were not correlated with shifts in either δ^{202}Hg or Δ^{199}Hg values ($r = 0.09$, $p = 0.65$ and $r = -0.08$, $p = 0.68$, respectively), making it unlikely that intermittent impacts from a single local source of anthropogenic emissions was the sole control on TGM isotopic composition throughout this study.

3.1.2. Mercury Isotopic Composition

The isotopic composition of daily atmospheric TGM samples was characterized by positive δ^{202}Hg values (0.39 to 1.43‰) and significant negative MIF of the odd-mass-number isotopes (mean Δ^{199}Hg = −0.22‰ ± 0.05‰ 1SD, $p < 0.001$ and mean Δ^{201}Hg = −0.19‰ ± 0.04‰ 1SD, $p < 0.001$; Table 2 and Figure 2). These δ^{202}Hg values (>1.0‰) are the highest reported to date for ambient

Global Biogeochemical Cycles 10.1002/2015GB005146

Table 2. Concentration and Isotopic Composition of Ambient Atmospheric Mercury (Total Gaseous Mercury, TGM) in a Coastal Urban-Industrial Region Near a Coal-Fired Power Plant in Pensacola, Florida, USA[a]

Day of Study	Start Date	Hg Concentration (ng/m^3)	n	δ^{204}Hg (‰)	2σ (‰)	δ^{202}Hg (‰)	2σ (‰)	δ^{201}Hg (‰)	2σ (‰)	δ^{200}Hg (‰)	2σ (‰)	δ^{199}Hg (‰)	2σ (‰)	Δ^{204}Hg (‰)	2σ (‰)	Δ^{201}Hg (‰)	2σ (‰)	Δ^{200}Hg (‰)	2σ (‰)	Δ^{199}Hg (‰)	2σ (‰)
1	100724	1.14	1	1.16	0.08	0.71	0.04	0.29	0.05	0.28	0.04	−0.07	0.04	0.10	0.04	−0.24	0.04	−0.07	0.04	−0.25	0.04
2	100725	1.16	1	1.35	0.08	0.91	0.04	0.46	0.05	0.35	0.04	−0.03	0.04	−0.01	0.04	−0.23	0.04	−0.10	0.04	−0.26	0.04
3	100726	1.02	2	1.40	0.08	0.87	0.04	0.45	0.05	0.42	0.04	0.02	0.04	0.10	0.04	−0.21	0.04	−0.02	0.04	−0.20	0.04
4	100727	1.00	1	1.43	0.08	0.82	0.04	0.48	0.05	0.29	0.04	−0.07	0.04	0.21	0.04	−0.14	0.04	−0.12	0.04	−0.27	0.04
5	100728	1.08	1	0.90	0.08	0.48	0.04	0.19	0.05	0.20	0.04	−0.09	0.04	0.18	0.04	−0.17	0.04	−0.04	0.04	−0.21	0.04
6	100729	1.11	1	1.19	0.08	0.66	0.04	0.32	0.05	0.29	0.04	−0.10	0.04	0.20	0.04	−0.18	0.04	−0.04	0.04	−0.27	0.04
7	100730	1.11	1	1.00	0.08	0.61	0.04	0.24	0.05	0.22	0.04	−0.13	0.04	0.10	0.04	−0.21	0.04	−0.09	0.04	−0.28	0.04
8	100731	1.26	1	1.10	0.08	0.69	0.04	0.30	0.05	0.28	0.04	−0.06	0.04	0.07	0.04	−0.22	0.04	−0.07	0.04	−0.23	0.04
9	100801	1.15	1	0.79	0.08	0.46	0.04	0.16	0.05	0.23	0.04	−0.01	0.04	0.12	0.04	−0.18	0.04	0.00	0.04	−0.12	0.04
10	100802	1.17	1	2.15	0.08	1.43	0.04	0.92	0.05	0.69	0.04	0.25	0.04	0.02	0.04	−0.16	0.04	−0.03	0.04	−0.11	0.04
11	100803	1.08	2	1.33	0.08	0.83	0.04	0.46	0.05	0.34	0.04	0.02	0.04	0.10	0.04	−0.16	0.04	−0.07	0.04	−0.19	0.04
12	100804	1.00	1	2.07	0.08	1.32	0.04	0.88	0.05	0.70	0.04	0.22	0.04	0.10	0.04	−0.11	0.04	0.03	0.04	−0.11	0.04
13	100805	1.06	1	1.51	0.08	1.00	0.04	0.57	0.05	0.42	0.04	0.01	0.04	0.02	0.04	−0.18	0.04	−0.08	0.04	−0.24	0.04
14	100806	0.84	1	0.71	0.08	0.39	0.04	0.05	0.05	0.07	0.04	−0.15	0.04	0.13	0.04	−0.24	0.04	−0.12	0.04	−0.25	0.04
15	100807	1.23	1	1.70	0.08	1.01	0.04	0.65	0.05	0.43	0.04	0.05	0.04	0.20	0.04	−0.11	0.04	−0.07	0.04	−0.21	0.04
16	100808	1.13	1	2.01	0.08	1.28	0.04	0.77	0.05	0.58	0.04	0.10	0.04	0.10	0.04	−0.19	0.04	−0.06	0.04	−0.23	0.04
17	100809	1.04	1	1.83	0.08	1.02	0.04	0.65	0.05	0.48	0.04	0.12	0.04	0.30	0.04	−0.12	0.04	−0.04	0.04	−0.13	0.04
18	100810	0.99	1	1.33	0.08	0.77	0.04	0.39	0.05	0.34	0.04	−0.05	0.04	0.19	0.04	−0.19	0.04	−0.05	0.04	−0.25	0.04
19	100811	1.05	1	1.49	0.08	0.91	0.04	0.50	0.05	0.34	0.04	−0.08	0.04	0.14	0.04	−0.18	0.04	−0.11	0.04	−0.31	0.04
20	100812	1.07	1	1.86	0.08	1.18	0.04	0.71	0.05	0.56	0.04	0.11	0.04	0.10	0.04	−0.18	0.04	−0.04	0.04	−0.18	0.04
21	100813	1.08	1	1.12	0.08	0.71	0.04	0.34	0.05	0.29	0.04	−0.06	0.04	0.07	0.04	−0.19	0.04	−0.07	0.04	−0.23	0.04
22	100814	1.14	1	1.43	0.08	0.89	0.04	0.52	0.05	0.37	0.04	0.01	0.04	0.10	0.04	−0.15	0.04	−0.08	0.04	−0.22	0.04
23	100815	1.24	1	1.51	0.08	0.95	0.04	0.51	0.05	0.42	0.04	0.00	0.04	0.10	0.04	−0.20	0.04	−0.06	0.04	−0.24	0.04
24	100816	1.21	1	1.10	0.08	0.66	0.04	0.24	0.05	0.31	0.04	−0.04	0.04	0.11	0.04	−0.26	0.04	−0.03	0.04	−0.21	0.04
25	100817	1.21	1	1.05	0.08	0.58	0.04	0.13	0.05	0.19	0.04	−0.15	0.04	0.19	0.04	−0.30	0.04	−0.10	0.04	−0.30	0.04
26	100818	1.14	1	1.26	0.08	0.72	0.04	0.34	0.05	0.25	0.04	−0.12	0.04	0.18	0.04	−0.20	0.04	−0.11	0.04	−0.30	0.04
27	100819	1.16	1	1.19	0.08	0.74	0.04	0.39	0.05	0.32	0.04	−0.06	0.04	0.09	0.04	−0.17	0.04	−0.05	0.04	−0.25	0.04
28	100820	1.13	1	1.21	0.08	0.81	0.04	0.40	0.05	0.35	0.04	−0.03	0.04	0.00	0.04	−0.21	0.04	−0.06	0.04	−0.24	0.04
29	100821	1.26	1	1.49	0.08	0.88	0.04	0.38	0.05	0.41	0.04	−0.06	0.04	0.17	0.04	−0.28	0.04	−0.04	0.04	−0.28	0.04
30	100822	1.14	2	1.59	0.08	1.00	0.04	0.55	0.05	0.47	0.04	0.03	0.04	0.09	0.04	−0.21	0.04	−0.03	0.04	−0.22	0.04

[a]Each consecutive day of study shows the isotopic composition of atmospheric TGM collected over a 24 h period. Here n denotes the number of independent field replicates. The 2σ for all samples shows either the 2SD of average of session averages for UM-Almaden or the 2SE of average of session averages for procedural standards, whichever uncertainty was largest (see section 2.4). The start date is in YYMMDD format.

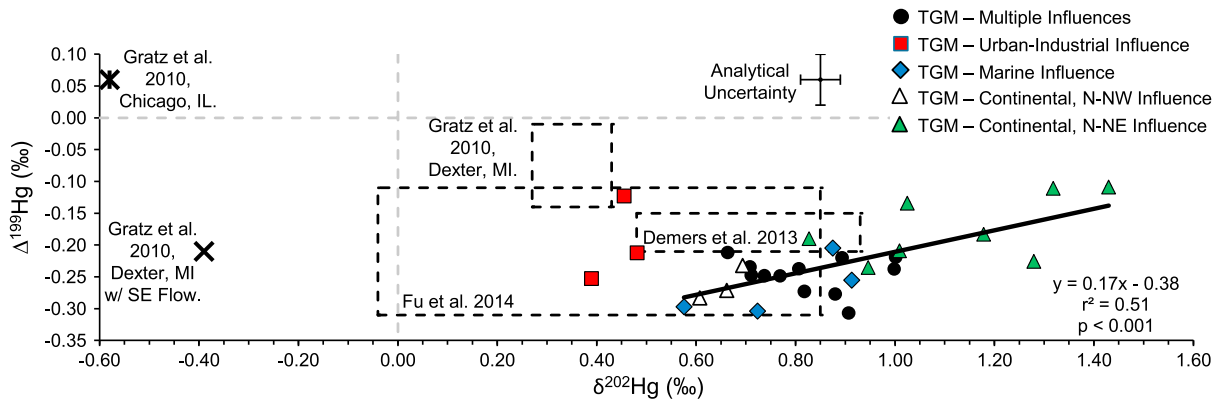

Figure 2. Isotopic composition of ambient atmospheric mercury (total gaseous mercury, TGM) in a coastal urban-industrial region near a coal-fired power plant in Pensacola, Florida, USA. MDF is shown by δ^{202}Hg (‰), and odd-mass-number MIF is shown by Δ^{199}Hg (‰). The isotopic compositions of each of the 24 h daily TGM samples that were predominantly impacted by identifiable influences, as determined by meteorological assessments, are shown with different symbols, as detailed in the legend. The analytical uncertainty of samples is represented by the 2SD of average of session averages for UM-Almaden or the 2SE of average of session averages for procedural standards, whichever uncertainty was largest (see section 2.4). The regression line excludes TGM samples determined to be influenced by emissions from urban-industrial regions. Gray dashed lines show zero values for δ^{202}Hg and Δ^{199}Hg. Dashed boxes show the range of mercury isotopic composition of TGM samples from other studies. The black cross and asterisk show samples influenced by urban-industrial regions reported in *Gratz et al.* [2010].

atmospheric TGM samples; only atmospheric TGM samples that have passed through the soil environment and undergone air-surface exchange are comparably high [*Demers et al.*, 2013].

Somewhat surprisingly, the isotopic composition of atmospheric TGM from this urban-industrial region in Florida was more similar to atmospheric TGM from non–urban-industrial regions of the Upper Midwest [*Gratz et al.*, 2010; *Demers et al.*, 2013] and the remote Pic du Midi Observatory, France [*Fu et al.*, 2014], than to TGM originating from other urban-industrial areas (mean δ^{202}Hg = −0.49‰ ± 0.13‰, 1SD and mean Δ^{199}Hg = −0.08‰ ± 0.19‰, 1SD; Figure 2) [*Gratz et al.*, 2010]. One previous study in the Gulf Coast region reported atmospheric samples with highly negative δ^{202}Hg values (−0.36 to −3.66‰) [*Rolison et al.*, 2013]; however, the sampling design in that study did not exclude aerosols, and thus, particulate-bound mercury from nearby anthropogenic sources may have influenced their results [*Blum et al.*, 2014]. In our study, TGM exhibited high variability in both δ^{202}Hg and Δ^{199}Hg values, similar to the range observed by *Gratz et al.* [2010] at a remote site occasionally impacted by air with a transport history influenced by urban-industrial regions, although our TGM data set was substantially shifted toward more positive δ^{202}Hg and more negative Δ^{199}Hg values (Figure 2). This high variability in isotopic composition may suggest that local and regional anthropogenic and background environmental sources of atmospheric mercury variably impact this coastal urban-industrial site (e.g., Figure 1).

It is difficult to decipher the influence of local and regional anthropogenic and background environmental sources contributing to ambient atmospheric mercury, in part, because the Hg isotopic composition of source emissions is poorly constrained. For example, the isotopic composition of mercury emissions from coal-fired power plants varies depending on source of feed coal, plant operating conditions, and use of air pollution control devices (APCDs). During 2009 and 2010, the coal combusted at the Crist power plant was primarily Appalachian Basin coal from Kentucky and West Virginia (73%) [*United States Energy Information Administration*, 2010]. Previous studies of North American coals have found that Appalachian Basin coals display negative δ^{202}Hg values (−0.88‰ ± 0.63‰ 1SD, n = 7) [*Biswas et al.*, 2008; *Sherman et al.*, 2012]. After GEM is released during coal combustion, fractionation of Hg isotopes during oxidation to GOM and incomplete removal of these oxidized Hg species by APDCs can modify the isotopic composition of emitted Hg relative to feed coal. *Sun et al.* [2013] estimated the isotopic composition of total stack emissions from coal-fired power plants (with ESPs only) to have δ^{202}Hg values ~0.3‰ higher than feed coal, with GOM δ^{202}Hg values ~0.1‰ lower than feed coal and GEM δ^{202}Hg values ~1.1‰ higher than feed coal [*Sun et al.*, 2014]. In 2010, the four boilers of the Crist power plant were all equipped with electrostatic precipitators (ESPs) and wet flue gas desulfurization units (WFGDs). The use of WFGD units is expected to remove nearly all GOM produced and likely promotes additional mercury removal though surface reactions that oxidize GEM [e.g., *Demers et al.*, 2013]. As a result, modeled Hg emissions from the Crist power plant were an estimated

92% GEM, 8% GOM, and < 1% PBM [*USEPA*, 2011a]. Removal of the oxidized species by WFGD would likely drive residual emitted GEM to higher δ^{202}Hg values. Thus, based on our estimate of feed coal composition and fractionation during oxidation and removal processes, GEM emissions from the Crist power plant would likely have δ^{202}Hg values at least as high as ~0.2‰. In-plume chemical reduction of up to ~50% of emitted GOM [*Landis et al.*, 2014] would likely drive GEM to lower δ^{202}Hg values. Overall, this would suggest that consistent with previous studies, local sources derived from urban-industrial regions and emissions from coal combustion would result in lower ambient atmospheric TGM δ^{202}Hg values compared to the more positive δ^{202}Hg values thought to represent background ambient atmospheric TGM [*Gratz et al.*, 2010; *Demers et al.*, 2013].

3.1.3. Diagnostic Ratios of MDF and MIF

The ratio of Δ^{199}Hg to δ^{202}Hg can be diagnostic of different volatilization pathways, most involving photochemistry and resulting from the magnetic isotope effect (e.g., see *Blum et al.* [2014, Figure 1] for a diagrammatic representation of these processes). For example, photochemical reduction of Hg(II) from aqueous solution in the presence of dissolved organic matter with nonsulfur-bearing ligands results in a Δ^{199}Hg/δ^{202}Hg ratio of 1.2 ± 0.07 (1SE) [*Bergquist and Blum*, 2007], whereas thiol ligands result in a ratio of about −0.80 [*Zheng and Hintelmann*, 2010a]. In contrast, equilibrium evaporation experiments between $Hg(0)_{liquid}$ and $Hg(0)_{gas}$ result in Δ^{199}Hg/δ^{202}Hg that falls on a line with a shallow slope of ~0.1, due to nuclear volume effects (NVE) [*Estrade et al.*, 2009; *Ghosh et al.*, 2013]. In our study, ambient atmospheric mercury falls along a Δ^{199}Hg/δ^{202}Hg line with a slope of 0.17 ± 0.03 (1SD, $r^2 = 0.51$, $p < 0.001$; Figure 2), similar to fractionation during evaporation experiments, but it could also be due to mixing between multiple sources of mercury with variable MIF and MDF (e.g., coal combustion, and photochemical reduction and oxidation processes in terrestrial, aquatic, and atmospheric environments). Although MIF signatures in coal would likely be conserved through combustion and removal by APCD units, MDF signatures would not be conserved [*Sun et al.*, 2013, 2014]. Therefore, Δ^{199}Hg/δ^{202}Hg ratios conserved within the feed coal would also not likely be observed in emissions from coal-fired power plants. Thus, diagnostic Δ^{199}Hg/δ^{202}Hg signatures would likely be obscured by the mixing of products from various biogeochemical reactions and contributions from multiple sources.

The ratio of Δ^{199}Hg to Δ^{201}Hg can also be diagnostic of fractionation processes. The Δ^{199}Hg/Δ^{201}Hg ratio of atmospheric TGM in this study falls on a line with a slope of 0.63 ± 0.19 (1SE, $p = 0.002$, $n = 30$); the 95% confidence interval of this slope ranged from 0.24 to 1.02 (supporting information Figure S1). Notably, the Δ^{199}Hg/Δ^{201}Hg ratio fell on a line with a slope of 0.89 ± 0.12 (1SE, $p < 0.001$, $n = 26$) for precipitation and atmospheric gaseous mercury in the Upper Midwest region [*Gratz et al.*, 2010], and in a study of world coals, Δ^{199}Hg/Δ^{201}Hg ratios fell on a line with a slope of ~1.1 ± 0.02 (1SE) [*Sun et al.*, 2014]. Based on experimental data, MIF due to the MIE occurring during photochemical reduction of Hg(II) from aqueous solutions in the presence of dissolved organic carbon is characterized by a Δ^{199}Hg/Δ^{201}Hg ratio of 1.00 ± 0.01(1SE) and photochemical degradation of MeHg yields a Δ^{199}Hg/Δ^{201}Hg ratio of 1.36 ± 0.04 (1SE) [*Bergquist and Blum*, 2007], whereas MIF due to the nuclear volume effect occurring during equilibrium evaporation experiments results in a Δ^{199}Hg/Δ^{201}Hg ratio of 1.59 ± 0.01 (1SE) [*Ghosh et al.*, 2013], and abiotic non-photochemical reduction of Hg(II) by dissolved organic matter and stannous chloride results in a Δ^{199}Hg/Δ^{201}Hg ratio of ~1.5–1.6 [*Zheng and Hintelmann*, 2010b]. These Δ^{199}Hg/Δ^{201}Hg ratios within natural samples are, however, difficult to determine accurately when MIF values are < ± 0.30‰ [*Blum et al.*, 2014], as they are in this study. Thus, despite high variability, the Δ^{199}Hg/Δ^{201}Hg ratio of TGM samples collected during this study is most similar to that produced during photochemical reduction of Hg(II) from aqueous solution, whether distally derived from the release of legacy sources during coal combustion or more proximally generated through photochemical reduction in the atmosphere, from terrestrial surfaces, or within the adjacent marine environment of the Gulf of Mexico.

3.1.4. MIF of Even-Mass-Number Isotopes

Atmospheric TGM was characterized by significant MIF of even-mass-number isotopes. The samples exhibited small negative Δ^{200}Hg values (−0.12‰ to 0.03‰) coupled with small positive Δ^{204}Hg values (−0.01‰ to 0.30‰), similar to previous studies [*Gratz et al.*, 2010; *Demers et al.*, 2013] (Figure 3). There was a significant relationship between Δ^{200}Hg and Δ^{199}Hg values (slope = 1.06 ± 0.19 (1SE), $r^2 = 0.54$, $p < 0.001$, $n = 30$) (supporting information Figure S1). *Gratz et al.* [2010] and *Demers et al.* [2013] also observed positive relationships between Δ^{200}Hg and Δ^{199}Hg values within combined TGM and precipitation data sets

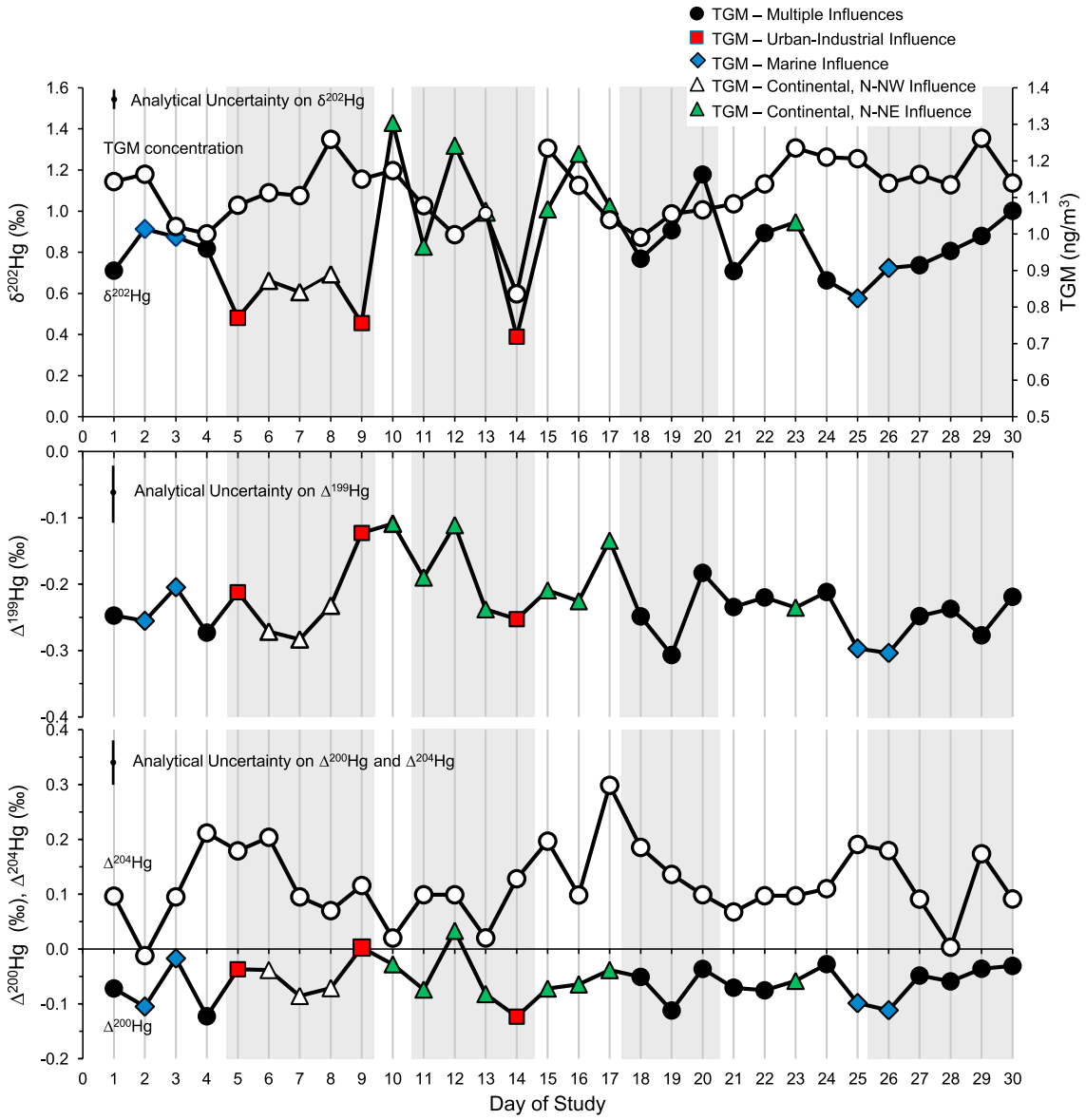

Figure 3. Stacked graphs showing the concentration and δ^{202}Hg, Δ^{199}Hg, Δ^{200}Hg, and Δ^{204}Hg values of ambient atmospheric mercury (total gaseous mercury, TGM) versus day of study, chronologically, in a coastal urban-industrial region near a coal-fired power plant in Pensacola, Florida, USA. The isotopic compositions of each of the 24 h daily TGM samples that were predominantly impacted by identifiable influences, as determined by meteorological assessments, are shown with different symbols, as detailed in the legend. We divided the 30 day study into eight meteorological periods based on synoptic-scale surface maps and 24 h back trajectories, as discussed in the text (see section 3.2.2); each of these periods is depicted by alternating shaded and nonshaded areas. The analytical uncertainty of samples is represented by the 2SD of average of session averages for UM-Almaden or the 2SE of average of session averages for procedural standards, whichever uncertainty was largest (see section 2.4).

but with greater slopes and more variance explained (1.87 ± 0.40 (1SE), $r^2 = 0.80$, $p < 0.001$, $n = 27$ and 2.39 ± 0.47 (1SE), $r^2 = 0.81$, $p = 0.002$, $n = 8$, respectively). As in other studies, we have not established a mechanistic explanation for these observations; however, they likely reflect a consistency in atmospheric sources and processes that generate the proportional isotopic effects observed in each study.

MIF of even-mass-number isotopes of Hg likely results from atmospheric processes, given that observations of even-mass-number MIF are most evident in precipitation and atmospheric gaseous mercury samples [e.g., *Gratz et al.*, 2010; *Chen et al.*, 2012; *Demers et al.*, 2013], and that these atmospheric pools typically have complementary values suggestive of heterogeneous liquid-gas phase reactions. *Chen et al.* [2012] suggested that self-shielding during photochemical reactions, which can fractionate Hg isotopes according to their

relative abundances, was the only mechanism identified that could potentially result in observed Δ^{200}Hg anomalies; however, the observed atmospheric fractionation patterns are not consistent with self-shielding in Hg vapor lamps [*Chen et al.*, 2012; *Mead et al.*, 2013]. *Chen et al.* [2012] further hypothesized that even-mass-number isotope anomalies were likely derived from redox reactions transforming Hg(0) to Hg(II) followed by scavenging onto droplets or particles during specific oxidation reactions, such as those involving ozone and sunlight, or halogen-enriched solid surfaces. The authors suggested that these reactions would predominantly occur at high altitudes and that long residence times of aerosols at high altitude could induce larger even-mass-number isotope anomalies associated with oxidized pools (GOM and PBM). *Chen et al.* [2012] observed very large even isotope anomalies in precipitation samples from Ontario, Canada (Δ^{200}Hg values from 0.21‰ to 1.24‰). Given that only a small fraction of the atmospheric TGM pool is oxidized, the larger complementary atmospheric Hg(0) pool would likely display only small negative ^{200}Hg anomalies [*Chen et al.*, 2012]. Nonetheless, if the hypotheses of *Chen et al.* [2012] are correct, this would imply that small negative ^{200}Hg anomalies within atmospheric TGM samples could be indicative of longer range transport from higher altitudes, whereas the lack of significant even-mass-number isotope anomalies might be suggestive of more localized emissions.

3.2. Meteorological Analyses and Criteria Pollutants

Mercury concentration and isotopic data suggest that local and regional anthropogenic and background environmental sources of mercury variably impacted this coastal urban-industrial site. However, mercury isotope systematics are not sufficiently established to allow for the specific identification of those sources based on isotopic data alone. Here we use assessments of criteria pollutants and local-scale, mesoscale, and synoptic-scale meteorological analyses to identify potential sources that may be driving the observed variations in isotopic composition of ambient atmospheric mercury. Further, we evaluate whether this data set is consistent with conceptual models put forth by previous work, in particular, that background ambient atmospheric mercury is represented by highly positive δ^{202}Hg values, whereas urban-industrial sources have lower δ^{202}Hg values.

3.2.1. Criteria Pollutants and Local-Scale Meteorology

As previously noted, there was no overall correlation between atmospheric TGM concentrations and δ^{202}Hg values. There was also no overall correlation between TGM δ^{202}Hg values and SO_2 or NO_x emissions from the Crist power plant ($r = 0.25$, $p = 0.18$ and $r = 0.04$, $p = 0.84$, respectively), or local ambient atmospheric concentrations of SO_2 ($r = -0.06$, $p = 0.75$). Based on measurements made at the Pensacola Airport (8 km south-southwest of our sampling site), we found no evidence that daily differences in average local surface wind speed and wind direction, including sea breeze effects, had an influence on TGM isotopic composition, although on-site collection of such data could improve this assessment in future studies. Linear regressions showed that the total daily precipitation amount measured neither at the TGM sampling site nor at the Pensacola Airport explained much of the variation in δ^{202}Hg values of atmospheric TGM ($r^2 = 0.12$ and $r^2 = 0.13$, respectively), and neither relationship had an associated slope value significantly different from zero at the 95% confidence level ($p = 0.063$ and $p = 0.051$, respectively). Thus, criteria pollutant and local-scale meteorological data provide no evidence that a single local source was consistently the predominant driver of TGM concentration or isotopic composition during this study.

3.2.2. Chronological Assessment of Synoptic-Scale and Mesoscale Meteorology

We divided our 30 day study into eight meteorological periods based on synoptic-scale surface maps and 24 h back trajectories (Figure 3). Here we chronologically summarize the meteorological conditions during each period and evaluate the influence of synoptic-scale and mesoscale meteorological parameters on the isotopic composition of ambient atmospheric mercury.

The first meteorological period (Days 1–4) was initially under the influence of a transient low-pressure system, with a weakening tropical depression moving onshore from the Gulf of Mexico. Through this period, there was also a cold front moving slowly from the midcontinent to the southeastern USA, remaining to the north of the Florida panhandle. The established daytime mixed layer depth averaged 1108 m, and the established nocturnal mixed layer depth averaged 550 m. Thus, meteorological conditions during this period were not conducive to the trapping of local pollutants near the ground surface. Based on back trajectories, air was transported to our sampling site by predominantly southerly flow from the Gulf of Mexico, swinging from southeasterly flow from over the Florida peninsula at the beginning of Day 1 to westerly flow along the

Gulf Coast at the end of Day 4. During this period, δ^{202}Hg values were tightly clustered (0.71 to 0.91‰), with the 2 days of solely marine influence displaying the most positive δ^{202}Hg values (0.87 to 0.91‰) (Table 2).

The second meteorological period (Days 5–9) was characterized by a transient high-pressure system, mostly centered over the Gulf Coast states, with a cold front slowly moving in from the north and becoming stationary across Arkansas, Mississippi, Alabama, and Georgia. The established daytime mixed layer depth averaged 1604 m, whereas the established nocturnal mixed layer depth averaged only 121 m and air arriving to our site at 0100 CDT (central daylight time) had been transported at an average maximum height of 157 m above ground level (agl) throughout the 24 h back trajectories. Thus, meteorological conditions during this period were somewhat stagnant and may have provided the potential for the trapping of local and regional pollutants near the ground surface, especially during the night. Based on back trajectories, air arriving at our sampling site was predominantly transported by north-northwesterly flows of continental origin during this period. However, Days 5 and 9 were more influenced by weaker, less consistent regional flows from along the western Gulf Coast (including the Mobile, Alabama, area). During this period, δ^{202}Hg values were also tightly clustered (0.46 to 0.69‰), with the weakest flows and greatest influence from the western Gulf Coast region on Day 5 and Day 9 associated with the least positive δ^{202}Hg values (0.46 to 0.48‰). These are two of the three lowest TGM δ^{202}Hg values measured in our study. Based on our meteorological assessments, these values appear to represent impacts from local to regional urban-industrial sources along the Gulf Coast to the west of our sampling site (Figure 1). This would be consistent with other studies that suggest urban-industrial areas contribute TGM with lower δ^{202}Hg values than do more rural background sites [*Gratz et al.*, 2010].

The next several meteorological periods (including Days 10–20) were more variable in their meteorology and ambient atmospheric mercury isotopic composition, and we discuss them in chronological order below. Notably, these periods encompass the seven atmospheric TGM samples with the highest δ^{202}Hg values (1.00 to 1.43‰).

The meteorology on Day 10 differed from the immediately preceding and subsequent periods, and the resulting δ^{202}Hg value of TGM sampled on Day 10 (1.43‰) was the most positive measured in this study. During Day 10, the Florida panhandle was not influenced by either transient high-pressure or transient low-pressure systems, or the semipermanent Bermuda High. A weak cold front stretching across the states to the north became stationary as the day progressed, dissipating by 1900 CDT. Daytime and nocturnal back trajectories from one half the mixed layer depth indicated predominantly southeasterly flow from the Gulf of Mexico. Whereas back trajectories starting at both one half the mixed layer height and 2000 m agl showed transport of air from similar regions during Days 1 to 9, the back trajectories starting at 2000 m agl on Day 10 suggested transport of air from the northeast, opposite the southeasterly transport within the mixed layer. It is possible that directional shear at the top of the boundary layer could increase turbulence and promote the entrainment of air from the free troposphere into the planetary boundary layer. Mixed layer heights, air transport heights, and back trajectories with starting heights originating within the mixed layer did not differentiate this TGM sampling period from others. However, the back trajectories starting at 2000 m agl and originating from the northeast may, in part, be driving the highly positive δ^{202}Hg value of the TGM sample on Day 10.

Days 11–14 were characterized by similar synoptic-scale meteorology as Days 5–9, with a transient high-pressure system centered in Louisiana on Day 11 that moved east-southeast into the Gulf of Mexico as a cold front moved slowly into the region from midcontinent and became stationary to the north across Louisiana, Mississippi, Alabama, and Georgia. During Days 11–13, back trajectories from the mixed layer suggest that air was transported to our site by southeasterly flows predominantly from over the Gulf of Mexico and to a lesser extent along the west Gulf Coast (excluding the Mobile region). However, back trajectories starting at 2000 m agl again suggested that air was transported from the northeast, similar to Day 10, and atmospheric TGM samples collected during these days also had high δ^{202}Hg values (0.83 to 1.32‰). This emerging association between northeasterly flows and more positive δ^{202}Hg values could be a regional continental signal arising from air-surface exchange of ambient atmospheric mercury moving across forests of the Appalachian Mountains to the northeast (which could increase δ^{202}Hg values) [*Demers et al.*, 2013] or, given the higher-altitude nature of these flows, may also indicate the entrainment of ambient atmospheric mercury from the global atmospheric reservoir.

Day 14 provides a salient contrast to this proposed influence of the global atmospheric mercury reservoir on the isotopic composition of TGM. Within the same synoptic meteorological regime as Days 11–13, back trajectories within the mixed layer on Day 14 shifted to indicate predominantly westerly transport along the Gulf Coast, with back trajectories from 2000 m agl also shifting to indicate air transport from the west-northwest. This shift to westerly back trajectories was associated with a large decrease in δ^{202}Hg to the lowest value observed in this study (0.39‰). Similar to Days 5 and 9 (δ^{202}Hg = 0.46 to 0.48‰), we suggest that this low value resulted from contributions of TGM from local- and regional-scale anthropogenic emissions along the Gulf Coast.

Meteorological conditions during Days 15–17, similar to Day 10, were characterized by the absence of distinct synoptic-scale features. The Florida panhandle did not appear to be strongly influenced by transient high- or low-pressure systems. Back trajectories from within the mixed layer suggest a variable origin of the air being transported to our site during this period, ranging from west-northwesterly flows from midcontinental and Gulf Coast regions to easterly flows from over the Florida panhandle. However, similar to Days 10–13 (with TGM δ^{202}Hg values of 0.83 to 1.43‰), back trajectories from 2000 m agl suggested predominantly north-northeasterly flows and were also associated with similarly positive δ^{202}Hg values (1.01 to 1.28‰).

Days 18–20 were characterized by the development of a tropical depression in the Gulf of Mexico southeast of the Florida panhandle. The storm developed on Day 18 and moved northwest toward the Gulf Coast, strengthening on Day 19 and then weakening again on Day 20 as it moved overland along the Gulf Coast west of the Florida panhandle. Back trajectories from within the mixed layer and starting at 2000 m agl on Days 18 and 19 suggest east-southeasterly flows from the Atlantic Ocean over the Florida peninsula and across the southeast Gulf Coast. These flows were associated with δ^{202}Hg values (0.77 to 0.91‰) similar to those observed during Days 1–4 (0.71 to 0.91‰). Thus, these data provide additional evidence that moderately positive TGM δ^{202}Hg values measured at this site may arise from air transport over marine environments. On Day 20, back trajectories from the mixed layer and from 2000 m agl suggest that south-southwesterly air transport from the Gulf of Mexico impacted our site. This was the only day with a TGM δ^{202}Hg value $>$ 1.00‰ (i.e., 1.18‰) that did not coincide with high-altitude flows from the north-northeast.

Synoptic features during the next meteorological period (Days 21–25) included a progressively weakening transient high-pressure system over the Gulf of Mexico and a weak transient low-pressure system that moved into the Gulf Coast region from the north. Slow-moving cold fronts from the north and northwest became stationary as they moved into the Gulf Coast region, just north of the Florida panhandle. During Days 21–23, the established daytime mixed layer depth averaged 918 m agl, whereas the established nocturnal mixed layer depth averaged only 262 m agl and air arriving to our site at 0100 CDT had been transported at an average maximum height of only 131 m agl throughout the 24 h back trajectories. Thus, meteorological conditions at the beginning of this period may have been conducive to trapping of local and regional pollutants near the ground surface, especially during the nighttime. Back trajectories from within the mixed layer on Days 21 and 22 suggest that air was transported to our site by westerly flows along the west Gulf Coast, including the Mobile, Alabama, region. On Day 23, westerly flows shifted to north/northeasterly flows within the mixed layer. Similarly, back trajectories from 2000 m agl showed a shift in higher-altitude flows from north-northwesterly to north-northeasterly over this same period. Coinciding with these shifts from west-northwesterly to more north-northeasterly flows, especially at high altitudes, was a shift in δ^{202}Hg values from 0.71‰ to 0.95‰, likely influenced by more north-northeasterly flows, similar to Days 10–13 and 15–17.

By Days 24–25, the weak transient high-pressure systems had completely dissipated and a weak low-pressure system remained to the west-southwest of the Pensacola sampling site. The average established daytime mixed layer depth (1160 m agl), the average established nocturnal mixed layer depth (550 m agl), and the 1300 CDT and 0100 CDT average maximum air transport heights (868 m and 350 m, respectively) were all similar to those observed under similar meteorological conditions during Days 1–4. During this period, back trajectories suggest that air was transported to our site by predominantly southerly flows from over the Gulf of Mexico. This predominantly marine-influenced ambient atmospheric mercury displayed δ^{202}Hg values of 0.58 to 0.66‰ that were slightly lower than those observed under similar meteorological conditions during Days 1–4 (0.83 ± 0.09‰, 1SD).

The final meteorological period (Days 26–30) was characterized by weak transient high-pressure systems centered in the Gulf of Mexico, with intermittent influence from the semipermanent Bermuda High to the

west of the Florida peninsula, and a stationary front extending across the southeastern USA north of the Florida panhandle. The established daytime mixed layer depth averaged 1035 m agl. The established nocturnal mixed layer depth averaged 298 m agl, with air arriving at our site at 0100 CDT having been transported at an average maximum height of 154 m agl throughout the 24 h back trajectories. Thus, similar to Days 5–9, meteorological conditions during this period were somewhat stagnant and may have provided the potential for the trapping of local and regional pollutants near the ground surface, especially during the nighttime. Based on back trajectories from within the mixed layer and starting at 2000 m agl, the origin of air transported to our site shifted systematically during this period, as did the isotopic composition of ambient atmospheric mercury. On Day 26, back trajectories suggest that air was predominantly transported to our site by south-southwesterly flows originating from the Gulf of Mexico, with ambient atmospheric mercury composition characterized by a δ^{202}Hg value of 0.72‰, similar to the average marine-derived ambient atmospheric mercury isotopic composition within this study (δ^{202}Hg = 0.77 ± 0.15‰, 1SD, n = 4). During Days 27–28, air was transported to our site by more westerly flows along the Gulf Coast as determined by back trajectories starting within the mixed layer, but by more north-northwesterly flows from the midcontinent as determined by back trajectories starting at 2000 m agl. During these days, the atmospheric TGM δ^{202}Hg values ranged from 0.74 to 0.81‰, values that are more consistent with north-northwesterly continental flows (δ^{202}Hg = 0.65 ± 0.04‰, 1SD) than with westerly flows from along the urban-industrial western Gulf Coast region (δ^{202}Hg = 0.44 ± 0.05‰, 1SD). During Day 29–30, back trajectories originating from within the mixed layer and at 2000 m suggested that air was transported to the sampling site under more north-northwesterly flows from the midcontinent, resulting in δ^{202}Hg values ranging from 0.88 to 1.00‰. These flow conditions and δ^{202}Hg values suggest a diminished influence of emissions from the urban-industrial western Gulf Coast region.

4. Integrated Synthesis of Hg Isotope Systematics and Meteorological Analyses

Synoptic-scale and mesoscale meteorology suggested four broadly discernible influences on the isotopic composition of TGM in this coastal urban-industrial region: (1) local and regional urban-industrial anthropogenic emissions, (2) marine-influenced sources derived from the Gulf of Mexico, (3) continental sources associated with north-northwesterly flows from within the mixed layer, and (4) continental sources associated with north-northeasterly flows at higher altitudes (i.e., 2000 m agl). Although mercury isotope systematics suggested that multiple sources likely impacted many of the 24 h ambient TGM samples, we were able to identify subsets of samples that typified each of these meteorologically derived influences in order to quantify the isotopic composition of atmospheric TGM associated with each.

The influence of local to regional urban-industrial anthropogenic emissions was dominant on Days 5, 9, and 14. On these days, air was transported by westerly flows across the urban-industrial Gulf Coast region and transient high-pressure systems provided the potential for anthropogenic emissions to be trapped near the ground surface. Under these conditions, the incorporation of local to regional anthropogenic emissions was likely responsible for the lowest atmospheric TGM δ^{202}Hg values observed during this study (mean δ^{202}Hg = 0.44 ± 0.05‰, 1SD, n = 3).

The isotopic composition of atmospheric TGM on days dominated by marine-influenced sources (Days 2, 3, 25, and 26; mean δ^{202}Hg = 0.77 ± 0.15‰, 1SD, n = 4) or north-northwesterly continental-influenced sources derived from the mixed layer (Days 6–8; mean δ^{202}Hg = 0.65 ± 0.04‰, 1SD, n = 3) exhibited δ^{202}Hg values that were intermediate between urban-industrial emissions and more positive δ^{202}Hg values typical of non–urban-industrial regions (see section 3.2.2). It is possible that these intermediate values simply result from mixing between local-regional anthropogenic emissions and the global atmospheric mercury pool. However, the isotopic composition of these samples did not fall along a simple mixing line between urban-industrial impacted samples and those associated with north-northeasterly flows (Figure 2). We speculate that the slightly more negative Δ^{199}Hg values of these marine and north-northwesterly derived sources (mean Δ^{199}Hg = −0.27 ± 0.05, 1SD, n = 4 and −0.26 ± 0.03, 1SD, n = 3, respectively) could suggest the incorporation of mercury that was photochemically reduced and reemitted from terrestrial and marine surfaces. It is also interesting that nearly all of the samples displaying Δ^{200}Hg values ≤ −0.10‰ were associated with marine-derived air (i.e., five out of six samples; mean Δ^{200}Hg = −0.11 ± 0.01‰, 1SD). As previously discussed, these even-mass-number MIF signatures are hypothesized to arise at high altitudes within the global

atmospheric mercury pool from heterogeneous liquid-gas phase reactions involving ozone and sunlight, or halogen-enriched surfaces [*Chen et al.*, 2012]. Thus, MIF of even-mass-number isotopes within the marine-derived samples may suggest the influence of the background global atmospheric mercury pool, or that Δ^{200}Hg anomalies could also be generated at the atmospheric-marine interface. Ultimately, the influence of reemissions on the isotopic composition of ambient atmospheric mercury remains unclear.

Continental-derived air transported at higher altitudes (e.g., 2000 m agl) via north-northeasterly flows appears to be associated with more positive δ^{202}Hg values (Days 10–13, 15–17, and 23; mean δ^{202}Hg = 1.10 ± 0.21, 1SD, n = 8). It is possible that higher-altitude air is simply more representative of the background global atmospheric mercury pool; however, observations of even MIF may place additional constraints on this interpretation. As described above, *Chen et al.* [2012] suggested that MIF of even-mass-number isotopes is generated at high altitudes within the background global atmospheric mercury pool (see section 3.1.4), and this may be helpful for identifying air that contributes predominantly background ambient atmospheric mercury. However, in this study, the atmospheric TGM samples collected under north-northeasterly flow conditions did not have Δ^{200}Hg values consistently different from zero, averaging only −0.05 ± 0.04‰ (1SD, n = 8). It is possible that this north-northeasterly flow could have delivered mercury from the background global atmospheric mercury pool that was then entrained within the planetary boundary layer and mixed with local to regional anthropogenic emissions (Figure 1). Such mixing of sources could reduce the characteristic even-mass-number MIF signatures derived from the global atmospheric mercury pool, as similarly discussed by *Wang et al.* [2015] to explain Δ^{200}Hg values in precipitation samples impacted by anthropogenic emissions in China. However, this would also likely drive δ^{202}Hg to lower values, which is counter to our observations. It is possible that surface exchange of ambient atmospheric mercury moving across forested landscapes of the Appalachian Mountains, or the > 250 km forested fetch to the northeast of the sampling site (Figure 1), could result in the highly positive δ^{202}Hg values observed [*Demers et al.*, 2013]. Given that δ^{202}Hg values associated with higher-altitude north-northeasterly flows ranged from 0.83 to 1.43‰, both of these mechanisms, and perhaps others as well, may have had some influence on the isotopic composition of atmospheric TGM observed at the sampling site.

One overarching question regarding the application of stable mercury isotope techniques to source identification and attribution is the validity of the emerging conceptual model that TGM samples with low δ^{202}Hg values represent the impact of anthropogenic emissions and more positive δ^{202}Hg values represent the influence of the background global atmospheric mercury pool. In this study within the Gulf Coast region, and similar to previous studies in the Upper Midwest [*Gratz et al.*, 2010; *Demers et al.*, 2013], nonpoint source-impacted samples had higher δ^{202}Hg values than samples impacted by urban-industrial emissions, with a difference in δ^{202}Hg values of at least 0.75‰. However, the range of δ^{202}Hg values, especially among samples that are not impacted by anthropogenic sources, is large and appears to be regionally influenced (Figure 2). It is interesting that the highest-altitude, and arguably the most remote, ambient atmospheric mercury sampling site (Pic du Midi, France) [*Fu et al.*, 2014] exhibited δ^{202}Hg values that ranged from slightly negative (akin to anthropogenic impacts) to moderately positive (δ^{202}Hg = −0.04 to 0.85‰), but did not approach the highest positive δ^{202}Hg values observed in northern Wisconsin, USA [*Demers et al.*, 2013], or those associated with north-northeasterly flows within this study (Figure 2). Thus, we suggest a modification of the emerging paradigm regarding mercury isotope systematics of ambient atmospheric mercury. We hypothesize that the background global atmospheric mercury pool is characterized by moderately positive δ^{202}Hg values; that urban-industrial emissions drive the isotopic composition of ambient atmospheric mercury toward lower δ^{202}Hg values; and that air-surface exchange dynamics across terrestrial ecosystems drive the isotopic composition of ambient atmospheric mercury toward higher positive δ^{202}Hg values. We further suggest that MIF of both even-mass-number and odd-mass-number isotopes, likely generated by photochemical reactions either in the atmosphere or during reemission from terrestrial and aquatic ecosystems, can be obscured by mixing with anthropogenic emissions of mercury having different MIF signatures.

5. Implications for Future Research

Despite advances in our conceptual understanding of the global biogeochemical cycling of mercury, the isotopic composition of atmospheric pools and anthropogenic emissions of mercury remain poorly constrained. Future research should endeavor to better isolate and characterize the isotopic composition

of the global atmospheric mercury reservoir, reemissions of mercury from terrestrial and marine surfaces, and key anthropogenic sources including coal combustion, artisanal gold mining, metals production, and cement manufacturing. Furthermore, assessing the species-specific isotopic composition of GEM and GOM could provide additional information regarding atmospheric processes and the identification of sources. Only by better constraining the end member sources and fractionation processes that regulate the isotopic signature of ambient atmospheric mercury can we improve our ability to identify, track, and attribute the sources that contribute to atmospheric mercury at local, regional, and global scales.

Acknowledgments

All atmospheric mercury concentration and isotope ratio data are reported in Tables 1, 2, and S1. All criteria pollutant data (SO_2 and NO_x emissions, and atmospheric SO_2 concentrations) and meteorological data are available from their original sources, as cited in the text. This research was made possible through funding from the Florida Department of Environmental Protection (contract SP673) and by the extraordinary lifetime achievements of the late Gerald J. Keeler. We thank James Barres of the University of Michigan Air Quality Laboratory for his assistance with field sampling equipment. Naima Hall, Matthew Salvadori, Emily Thomas, and Tyler Osburn provided additional logistical and field support. We thank Marcus W. Johnson of the UM Biogeochemistry and Environmental Isotope Geochemistry Laboratory for his analytical assistance. Sarah North, Erin Lower, and Jonathon Syrek provided additional assistance in the laboratory. We thank Jane M. Caffrey for her assistance in establishing site access at the University of West Florida.

References

Amos, H. M., D. J. Jacob, D. G. Streets, and E. M. Sunderland (2013), Legacy impacts of all-time anthropogenic emissions on the global mercury cycle, *Global Biogeochem. Cycles*, *27*, 410–421, doi:10.1002/gbc.20040.

Bergquist, B. A., and J. D. Blum (2007), Mass-dependent and -independent fractionation of Hg isotopes by photoreduction in aquatic systems, *Science*, *318*, 417–420, doi:10.1126/science.1148050.

Bergquist, R. A., and J. D. Blum (2009), The odds and evens of mercury isotopes: Applications of mass-dependent and mass-independent isotope fractionation, *Elements*, *5*, 353–357, doi:10.2113/gselements.5.6.353.

Biswas, A., J. D. Blum, B. A. Bergquist, G. J. Keeler, and Z. Q. Xie (2008), Natural mercury isotope variation in coal deposits and organic soils, *Environ. Sci. Technol.*, *42*, 8303–8309, doi:10.1021/es801444b.

Blum, J. D., and B. A. Bergquist (2007), Reporting of variations in the natural isotopic composition of mercury, *Anal. Bioanal. Chem.*, *388*, 353–359, doi:10.1007/s00216-007-1236-9.

Blum, J. D., L. S. Sherman, and M. W. Johnson (2014), Mercury isotopes in Earth and environmental sciences, *Annu. Rev. Earth Planet. Sci.*, *42*, 249–269, doi:10.1146/annurev-earth-050212-124107.

Butler, T. J., M. D. Cohen, F. M. Vermeylen, G. E. Likens, D. Schmeltz, and R. S. Artz (2008), Regional precipitation mercury trends in the eastern USA, 1998–2005: Declines in the Northeast and Midwest, no trend in the Southeast, *Atmos. Environ.*, *42*, 1582–1592, doi:10.1016/j.atmosenv.2007.10.084.

Carpi, A. (1997), Mercury from combustion sources: A review of the chemical species emitted and their transport in the atmosphere, *Water, Air, Soil Pollut.*, *98*, 241–254, doi:10.1007/BF02047037.

Chen, J. B., H. Hintelmann, X. B. Feng, and B. Dimock (2012), Unusual fractionation of both odd and even mercury isotopes in precipitation from Peterborough, ON, Canada, *Geochim. Cosmochim. Acta*, *90*, 33–46, doi:10.1016/j.gca.2012.05.005.

Demers, J. D., J. D. Blum, and D. R. Zak (2013), Mercury isotopes in a forested ecosystem: Implications for air-surface exchange dynamics and the global mercury cycle, *Global Biogeochem. Cycles*, *27*, 222–238, doi:10.1002/gbc.20021.

Draxler, R. R., and G. D. Rolph (2010), HYSPLIT (HYbrid Single-Particle Langrangian Integrated Trajectory) Model, National Oceanographic and Atmospheric Science Administration, Air Resources Laboratory website http://ready.arl.noaa.gov/HYSPLIT.php, NOAA Air Resources Laboratory, College Park, Md., Accessed July 2014.

Dvonch, J. T., J. R. Graney, G. J. Keeler, and R. K. Stevens (1999), Use of elemental tracers to source apportion mercury in South Florida precipitation, *Environ. Sci. Technol.*, *33*, 4522–4527, doi:10.1021/es9903678.

Dvonch, J. T., G. J. Keeler, and F. J. Marsik (2005), The influence of meteorological conditions on the wet deposition of mercury in southern Florida, *J. Appl. Meteorol.*, *44*, 1421–1435, doi:10.1175/JAM2272.1.

Estrade, N., J. Carignan, J. E. Sonke, and O. F. X. Donard (2009), Mercury isotope fractionation during liquid–vapor evaporation experiments, *Geochim. Cosmochim. Acta*, *73*, 2693–2711, doi:10.1016/j.gca.2009.01.024.

Fu, X. W., L. E. Heimburger, and J. E. Sonke (2014), Collection of atmospheric gaseous mercury for stable isotope analysis using iodine- and chlorine-impregnated activated carbon traps, *J. Anal. Atom. Spectrom.*, *29*, 841–852, doi:10.1039/c3ja50356a.

Ghosh, S., E. A. Schauble, G. Couloume, J. D. Blum, and B. A. Bergquist (2013), Estimation of nuclear volume dependent fractionation of mercury isotopes in equilibrium liquid-vapor evaporation experiments, *Chem. Geol.*, doi:10.1016/j.chemgeo.2012.01.008.

Graney, J. R., J. T. Dvonch, and G. J. Keeler (2004), Use of multi-element tracers to source apportion mercury in South Florida aerosols, *Atmos. Environ.*, *38*, 1715–1726, doi:10.1016/j.atmosenv.2003.12.018.

Gratz, L. E., and G. J. Keeler (2011), Sources of mercury in precipitation to Underhill, VT, *Atmos. Environ.*, *45*, 5440–5449, doi:10.1016/j.atmosenv.2011.07.001.

Gratz, L. E., G. J. Keeler, J. D. Blum, and L. S. Sherman (2010), Isotopic composition and fractionation of mercury in Great Lakes precipitation and ambient air, *Environ. Sci. Technol.*, *44*, 7764–7770, doi:10.1021/es100383w.

Gratz, L. E., G. J. Keeler, F. J. Marsik, J. A. Barres, and J. T. Dvonch (2013a), Atmospheric transport of speciated mercury across southern Lake Michigan: Influence from emission sources in the Chicago/Gary urban area, *Sci. Total Environ.*, *448*, 84–95, doi:10.1016/j.scitotenv.2012.08.076.

Gratz, L. E., G. J. Keeler, M. Morishita, J. A. Barres, and J. T. Dvonch (2013b), Assessing the emission sources of atmospheric mercury in wet deposition across Illinois, *Sci. Total Environ.*, *448*, 120–131, doi:10.1016/j.scitotenv.2012.11.011.

Keeler, G., G. Glinsorn, and N. Pirrone (1995), Particulate mercury in the atmosphere: Its significance, transport, transformation and sources, *Water, Air, Soil Pollut.*, *80*, 159–168, doi:10.1007/BF01189664.

Landis, M. S., and G. J. Keeler (2002), Atmospheric mercury deposition to Lake Michigan during the Lake Michigan Mass Balance Study, *Environ. Sci. Technol.*, *36*, 4518–4524, doi:10.1021/es011217b.

Landis, M. S., J. V. Ryan, A. F. H. ter Schure, and D. Laudal (2014), Behavior of mercury emissions from a commercial coal-fired power plant: The relationship between stack speciation and near-field plume measurements, *Environ. Sci. Technol.*, *48*, 13,540–13,548, doi:10.1021/es500783t.

Lindberg, S. E., and W. J. Stratton (1998), Atmospheric mercury speciation: Concentrations and behavior of reactive gaseous mercury in ambient air, *Environ. Sci. Technol.*, *32*, 49–57, doi:10.1021/es970546u.

Mead, C., J. R. Lyons, T. M. Johnson, and A. D. Anbar (2013), Unique Hg stable isotope signatures of compact fluorescent lamp-sourced Hg, *Environ. Sci. Technol.*, *47*, 2542–2547, doi:10.1021/es303940p.

NOAA (2014a), National Climate Data Center, Climate Data Online. [Available at http://ncdc.noaa.gov/cdo-web, Accessed June 2014.]

NOAA (2014b), National Weather Service, National Centers for Environmental Prediction, Hydrometeorological Prediction Center. [Availble at http://www.wpc.ncep.noaa.gov/dailywxmap/index.html, Accessed June 2014.]

NOAA (2014c), National Weather Service, NWS DIFAX Weather Map Archive. [Available at http://archive.atmos.colostate.edu. Accessed June 2014.]

Pacyna, E. G., J. M. Pacyna, F. Steenhuisen, and S. Wilson (2006), Global anthropogenic mercury emission inventory for 2000, *Atmos. Environ.*, *40*, 4048–4063, doi:10.1016/j.atmosenv.2006.03.041.

Pirrone, N., et al. (2009), Global mercury emissions to the atmosphere from natural and anthropogenic sources, in *Mercury Fate and Transport in the Global Atmosphere: Emissions, Measurements and Models*, pp. 3–49, Springer, New York, doi:10.1007/978-0-387-93958-2_1.

Pirrone, N., et al. (2010), Global mercury emissions to the atmosphere from anthropogenic and natural sources, *Atmos. Chem. Phys.*, *10*, 5951–5964, doi:10.5194/acp-10-5951-2010.

Rolison, J. M., W. M. Landing, W. Luke, M. Cohen, and V. J. M. Salters (2013), Isotopic composition of species-specific atmospheric Hg in a coastal environment, *Chem. Geol.*, *336*, 37–49, doi:10.1016/j.chemgeo.2012.10.007.

Schroeder, W. H., and J. Munthe (1998), Atmospheric mercury: An overview, *Atmos. Environ.*, *32*, 809–822, doi:10.1016/S1352-2310(97)00293-8.

Selin, N. E. (2009), Global biogeochemical cycling of mercury: A review, *Annu. Rev. Environ. Resour.*, *34*, 43–63, doi:10.1146/annurev.environ.051308.084314.

Selin, N. E., and D. J. Jacob (2008), Seasonal and spatial patterns of mercury wet deposition in the United States: Constraints on the contribution from North American anthropogenic sources, *Atmos. Environ.*, *42*, 5193–5204, doi:10.1016/j.atmosenv.2008.02.069.

Sherman, L. S., J. D. Blum, G. J. Keeler, J. D. Demers, and J. T. Dvonch (2012), Investigation of local mercury deposition from a coal-fired power plant using mercury isotopes, *Environ. Sci. Technol.*, *46*, 382–390, doi:10.1021/es202793c.

Sherman, L. S., J. D. Blum, J. T. Dvonch, L. E. Gratz, and M. S. Landis (2015), The use of Pb, Sr, and Hg isotopes in Great Lakes precipitation as a tool for pollution source attribution, *Sci. Total Environ.*, *502*, 362–374, doi:10.1016/j.scitotenv.2014.09.034.

Sporl, R., L. Belo, K. Shah, R. Stanger, R. Giniyatullin, J. Maier, T. Wall, and G. Scheffknecht (2014), Mercury emissions and removal by ash in coal-fired oxy-fuel combustion, *Energy Fuel*, *28*, 123–135, doi:10.1021/ef4014604.

Srivastava, R. K., N. Hutson, B. Martin, F. Princiotta, and J. Staudt (2006), Control of mercury emissions from coal-fired in electric utility boilers, *Environ. Sci. Technol.*, *40*, 1385–1393, doi:10.1021/es062639u.

Sun, R. Y., L. E. Heimburger, J. E. Sonke, G. J. Liu, D. Amouroux, and S. Berail (2013), Mercury stable isotope fractionation in six utility boilers of two large coal-fired power plants, *Chem. Geol.*, *336*, 103–111, doi:10.1016/j.chemgeo.2012.10.055.

Sun, R. Y., J. E. Sonke, L. E. Heimburger, H. E. Belkin, G. J. Liu, D. Shome, E. Cukrowska, C. Liousse, O. S. Pokrovsky, and D. G. Streets (2014), Mercury stable isotope signatures of world coal deposits and historical coal combustion emissions, *Environ. Sci. Technol.*, *48*, 7660–7668, doi:10.1021/es501208a.

Telmer, K. M., and M. M. Veiga (2009), World emissions of mercury from artisanal and small scale gold mining, in *Mercury Fate and Transport in the Global Atmosphere: Emissions, Measurements and Models*, pp. 131–172, Springer, New York, doi:10.1007/978-0-387-93958-2_6.

Ticknor, J. L., H. Hsu-Kim, and M. A. Deshusses (2014), A robust framework to predict mercury speciation in combustion flue gases, *J. Hazard. Mater.*, *264*, 380–385, doi:10.1016/j.jhazmat.2013.10.052.

United Nations Environment Program (UNEP) (2013), *Global Mercury Assessment 2013: Sources, Emissions, Releases and Environmental Transport*, UNEP Chemicals Branch, Geneva, Switzerland.

United States Energy Information Administration (2010), Monthly Utility and Nonutility Fuel Receipts and Fuel Quality Data, United States Energy Information Administration EIA-923. [Available at http://www.eia.doe.gov/cneaf/electricity/page/eia423.html, Accessed June 2014.]

U.S. Environmental Protection Agency (1998), Method 1631: Measurement of mercury in water: Revision E, U.S. Environmental Protection Agency, Office of Water, Office of Science and Technology, Engineering and Analysis Division (4303), Washington, D. C.

U.S. Environmental Protection Agency (USEPA) (2011a), Electric generating utility mercury speciation profiles for the clear air mercury rule, U.S. Environmental Protection Agency, Office of Air Quality Planning and Standards, Air Quality Assessment Division, Emissions Inventory and Analysis Group., Research Triangle Park, N. C.

U.S. Environmental Protection Agency (USEPA) (2011b), National Emission Inventory (NEI). [Available at www.epa.gov/ttn/chief/net/2011inventory.html, Accessed May 2014.]

U.S. Environmental Protection Agency (2014a), Clean Air Markets: Air Markets Program Data. [Available at http://ampd.epa.gov/ampd, Accessed June 2014.]

U.S. Environmental Protection Agency (2014b), Mercury and Air Toxics Standards (MATS). [Available at www.epa.gov/airquality/powerplanttoxics/index.htm.]

Wang, Z., J. Chen, X. Feng, H. Hintelmann, S. Yuan, H. Cai, Q. Huang, S. Wang, and F. Wang (2015), Mass-dependent and mass-independent fractionation of mercury isotopes in precipitation from Guiyang, SW China, *C. R. Geosci.*, doi:10.1016/j.crte.2015.02.006.

Wilcox, J., E. Rupp, S. C. Ying, D. H. Lim, A. S. Negreira, A. Kirchofer, F. Feng, and K. Lee (2012), Mercury adsorption and oxidation in coal combustion and gasification processes, *Int. J. Coal Geol.*, *90*, 4–20, doi:10.1016/j.coal.2011.12.003.

Zhang, H., R. S. Yin, X. B. Feng, J. Sommar, C. W. N. Anderson, A. Sapkota, X. W. Fu, and T. Larssen (2013a), Atmospheric mercury inputs in montane soils increase with elevation: Evidence from mercury isotope signatures, *Sci. Rep.*, *3*, doi:10.1038/srep03322.

Zhang, L., M. Daukoru, S. Torkamani, S. X. Wang, J. M. Hao, and P. Biswas (2013b), Measurements of mercury speciation and fine particle size distribution on combustion of China coal seams, *Fuel*, *104*, 732–738, doi:10.1016/j.fuel.2012.06.069.

Zheng, W., and H. Hintelmann (2010a), Isotope fractionation of mercury during its photochemical reduction by low-molecular-weight organic compounds, *J. Phys. Chem. A*, *114*, 4246–4253, doi:10.1021/jp9111348.

Zheng, W., and H. Hintelmann (2010b), Nuclear field shift effect in isotope fractionation of mercury during abiotic reduction in the absence of light, *J. Phys. Chem. A*, *114*, 4238–4245, doi:10.1021/jp910353y.